ACI STRUCTURAL JOURNAL TECHNICAL PAPER

Title no. 109-S64

Simplified Method for Nonlinear Dynamic Analysis of Shear-Critical Frames

by Serhan Guner and Frank J. Vecchio

A nonlinear static analysis method was recently developed for the performance assessment of plane frames. The primary advantage of this method is its ability to accurately represent shear effects coupled with axial and flexural behaviors through a simple modeling approach suitable for large-scale applications. In this study, this method is further developed to enable a dynamic load analysis capability under impact, blast, and seismic loads. Newly developed and implemented formulations are presented. Among them are an explicit three-parameter time-step integration method, based on a total-load secant-stiffness formulation, and dynamic increase factor formulations for the consideration of strain rates. The method is applied to 11 previously tested specimens, subjected to impact and seismic loads, to examine its accuracy, reliability, and practicality. The method is found to simulate the overall experimental behaviors with a high degree of accuracy. Strengths, peak displacements, stiffnesses, damage, and failure modes (including shear-critical behaviors) and vibrational characteristics are calculated accurately. The method provides unconditional numerical stability and requires a fraction of the computation time demanded by micro finite element methods.

Keywords: blast; frame structures; impact; nonlinear analysis; secant stiffness; seismic; shear; strain rates; time-history analysis.

INTRODUCTION

The need for accurate analysis methods for impact and blast loads has increased considerably in recent years. Heightened levels of terrorist threat, for example, have resulted in strategic structures, such as government and commercial buildings, requiring design for blast and impact resilience. Currently available methods employed in practice are typically based on overly simplistic macro models, however, reducing each structural component to a single-degree-of-freedom system. One such method is proposed in UFC 3-340-02 (2008), a manual used in the past several decades for protective design. Unreliable and inaccurate responses obtained from such methods have been demonstrated in various studies, including El-Dakhakhni et al. (2009). On the other hand, micro finite element methods, such as LS-DYNA (2010) and ABAQUS (2010), are complex and computationally demanding, and thus have limited applicability to large frames encountered in practice. Moreover, the proper consideration of shear effects remains a major deficiency—even in the micro finite element methods—despite the fact that impact and blast loads tend to result in significant shear damage, as was observed by Saatci and Vecchio (2009a) and Li et al. (2010). Consequently, a significant need for analysis methods that lie between these two extremes while being able to accurately model shear effects remains.

For earthquake loads, research studies conducted in the past number of decades have clearly demonstrated the importance of ductility in the survival of frames under strong ground motions. Modern seismic design codes, such as ACI 318-11 (ACI Committee 318 2011), have thus incorporated stringent provisions requiring structures to be ductile and flexure-critical in their behaviors; however, many existing structures were constructed before the introduction of modern seismic design guidelines with nonductile and shear-critical details. Gunay and Mosalam (2010) provide examples of concrete- and shear-dominated failures observed after a recent earthquake. Consequently, there is an urgent need to perform safety assessments to identify and upgrade such structures. Currently available dynamic analysis methods, such as Perform3D (CSI 2006) and SeismoStruct (SeismoStruct 2010), however, typically neglect shear-related effects by default. This omission may result in grossly unconservative and unsafe response predictions.

Consideration of shear behavior with the available methods may be possible through the input of shear-force and shear-deformation responses for each member section; however, the determination of these responses is complex, time-consuming, and requires significant knowledge of shear analysis methods. Moreover, even when using an input shear hinge model, the flexural and shear responses become uncoupled; in reality, they are interdependent. Finally, academic methods, such as OpenSees (2012), may be employed to consider shear behavior, but such methods require significant modeling and computer programming experience and thus are mostly suitable for researchers only.

FOCUS OF CURRENT STUDY

An analysis method was recently developed by Guner and Vecchio (2010, 2011) for the nonlinear static analysis of plane frames. The method employs multi-degree-of-freedom distributed-plasticity frame analysis algorithms in a nonlinear mode based on an unbalanced force approach. The nonlinear sectional analysis algorithms provide a comprehensive and accurate representation of shear effects based on the disturbed stress field model (Vecchio 2000). The method considers significant second-order mechanisms, such as the membrane action, concrete out-of-plane confinement effects, and reinforcement dowel action.

The objective of this study is to further develop this static analysis method to enable a dynamic load analysis capability. The main focus is to accurately represent the coupled interaction between shear, flexural, and axial effects through a modeling approach suitable for large-scale applications found in practice. A second focus is to explicitly consider the effects of the rate of loading. In this vein, a literature review

ACI Structural Journal, V. 109, No. 5, September-October 2012.
MS No. S-2010-400.R2 received August 13, 2011, and reviewed under Institute publication policies. Pertinent discussion including author's closure, if any, will be published in the July-August 2013 *ACI Structural Journal* if the discussion is received by March 1, 2013.

ACI member **Serhan Guner** *is a Structural Engineer at Morrison Hershfield Limited, Toronto, ON, Canada. He received his PhD in 2008 from the University of Toronto, Toronto, ON, Canada. He is a member of Joint ACI-ASCE Committee 447, Finite Element Analysis of Reinforced Concrete Structures. His research interests include analysis and performance assessment of concrete structures, shear effects in concrete, and structural dynamics and response to extreme loads.*

Frank J. Vecchio, *FACI, is a Professor of civil engineering at the University of Toronto. He is a member of Joint ACI-ASCE Committees 441, Reinforced Concrete Columns, and 447, Finite Element Analysis of Reinforced Concrete Structures. He received the 1998 ACI Structural Research Award, the 1999 ACI Structural Engineer Award, and the 2011 ACI Wason Medal for Most Meritorious Paper. His research interests include advanced constitutive modeling and analysis of reinforced concrete, assessment and rehabilitation of structures, and response under extreme loads.*

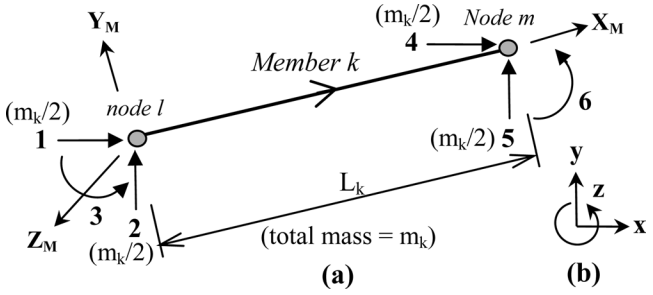

Fig. 1—Frame member proposed: (a) dynamic and mass degrees of freedom; and (b) global axes.

of the available strain rate models is conducted and the selected models are incorporated into the proposed method. A final focus is to present an approach through which a static analysis method can be modified for the consideration of dynamic loads in a total-load secant-stiffness formulation.

In this paper, only the new formulations implemented into the existing computer code VecTor5 (Guner and Vecchio 2008) are presented. The main framework of the analysis method is described in Guner and Vecchio (2010, 2011). Furthermore, verification studies are presented in this paper through the application of the proposed method, using only the default models and options, to 11 previously tested specimens subjected to impact loads and earthquake excitation. The structures examined include eight simply supported beams, two cantilever columns, and one shear-critical frame—comprising a total of 38 simulations. The experimental behaviors are compared to the computed responses. Important considerations in nonlinear modeling, such as the selection of a time-step length and integration method, are discussed.

RESEARCH SIGNIFICANCE

Although the prevalence of shear-dominated responses under impact, blast, and seismic loads is well-known, most currently available dynamic analysis methods neglect shear effects altogether. The methods that do consider shear influences are overly complex, requiring the input of sectional shear hystereses, and still tend to be inaccurate. This study describes the formulation and application of a nonlinear frame analysis method capable of inherently and accurately representing shear effects. Unlike most other methods, the developed method does not require the input of sectional response hystereses or other pre-analysis calculations and is suitable for practical applications ranging from seismic time-history to progressive collapse analyses.

MODIFICATIONS FOR DYNAMIC LOADING CONDITIONS

The analysis method being modified in this study was developed to perform static nonlinear analyses through the solution of Eq. (1). For a dynamic load analysis capability, the dynamic equation of motion of Eq. (2) must be constructed and solved.

$$\{u\} = [k]^{-1} \times \{p\} \tag{1}$$

$$m \times \ddot{u}(t) + c \times \dot{u}(t) + k \times u(t) = p(t) \tag{2}$$

In this study, Eq. (2) is condensed to the form of Eq. (1) so that it remains solvable by the analysis method developed for static loads. The following sections present the new formulations developed and implemented into the static analysis method.

GLOBAL FRAME ANALYSIS

A flowchart indicating the major steps in the global frame analysis is presented in Guner (2008, pp. 313-314), where the newly implemented algorithms are shown with the bold type and the modified algorithms are shown with the dotted lines.

Dynamic variables

Similar to the static case, three degrees of freedom are considered at each node: two translational and one rotational, as shown in Fig. 1. Furthermore, a lumped-mass approach is adopted with two translational degrees of freedom at each node.

In the analysis method being modified in this study, structural energy dissipation is considered primarily through the nonlinear concrete and reinforcing steel hysteresis models previously implemented by Guner and Vecchio (2011). For situations where the use of additional viscous damping is desired (for example, for frames with various nonstructural elements), two optional damping formulations are incorporated. The first formulation implemented employs Rayleigh damping (Rayleigh 1877), in which two damping ratios can be assigned to two vibration modes. The second formulation incorporated employs "alternative damping" and is useful when the exact specification of damping ratios to more than two vibration modes is needed. Details of both formulations can be found in Clough and Penzien (1993).

Four different types of dynamic loads are considered: base accelerations for seismic time-history analyses; impulse or force profiles for impact or blast analyses; initial mass velocities for impact analyses as employed in this study; and constant accelerations for, for instance, the simulation of gravity effects on masses in any type of dynamic analysis.

Numerical evaluation of dynamic equation of motion

An explicit time-step numerical integration method is adopted to solve the dynamic equation of motion. The first scheme implemented is Newmark's method (Newmark 1959) with two well-known special cases. The average constant acceleration method is an unconditionally stable procedure regardless of the time-step length used. Although more accurate, the linear acceleration method is a conditionally stable procedure requiring time-step lengths less than 0.5513 $\times T_N$, where T_N is the smallest modal period of the structure. This stability limit usually requires extremely small time-step

lengths, resulting in prohibitive computation times. Consequently, this method is more appropriate for highly dynamic and short-duration loads, such as impact or blast. The unconditionally stable constant acceleration method, on the other hand, is more appropriate for long-duration loads, such as with seismic loading, to reduce the computational demand.

Nonlinear analyses with either the average or linear acceleration method may require the use of a minimal amount of additional viscous damping for numerical stability; this need arises because when periods of oscillation exist, which are shorter than the integration time-step length, the structure tends to oscillate indefinitely once excited. One approach to prevent this is to determine the minimum damping ratio that will dampen out these higher frequencies, as was employed by Saatci and Vecchio (2009b). This approach, however, requires successive analyses and may require significant time and effort for a large-scale frame analysis. This may eventually lead the analyst to use higher damping ratios, typically resulting in unconservative responses with underestimated deflections. Note that the developed method considers the majority of structural energy dissipation through the concrete (Palermo and Vecchio 2003) and reinforcement hysteresis (Seckin 1981) models implemented.

To specifically address these difficulties, a third procedure, called Wilson's theta method (Wilson et al. 1973), was implemented; it is an unconditionally stable version of the linear acceleration method. In this method, the acceleration is assumed to vary linearly over an extended time-step length $\delta t = \theta \times \Delta t$. The resulting values at the end of the extended time step are then scaled back to the actual time step. This method provides inherent numerical damping within the solution, stabilizing the analysis by dampening out the responses of the modes with a shorter period than the time-step length used. It thereby eliminates the need for successive analyses. Consequently, Wilson's theta method is selected as the default option and is employed exclusively throughout this study.

Explicit solution based on total loads and secant stiffness

The nonlinear analysis method developed employs a total-load secant-stiffness formulation; therefore, the numerical solution of the dynamic equation of motion needs to be likewise evaluated. For this purpose, the original tangent-stiffness-based formulations of Newmark's method were modified to obtain a total-load secant-stiffness formulation after Saatci and Vecchio (2009b). In this modification, Wilson's theta method was also incorporated through the derivation of a three-parameter formulation, which is presented in the following.

The dynamic equation of motion can be expressed in terms of the total loads as follows

$$m \times \left(\ddot{u}_0 + \Delta\ddot{u}\right) + c \times \left(\dot{u}_0 + \Delta\dot{u}\right) + \bar{k}_1 \times u_1 = p_{stat} + p_1 \quad (3)$$

where p_{stat} is the constant static load; p is the dynamic load; and the subscript "0" represents values at the beginning of the time step and the subscript "1" represents values at the end of the time step. The incremental acceleration, velocity, and displacement are defined, respectively, as follows

$$\Delta\ddot{u} = \ddot{u}_1 - \ddot{u}_0; \qquad \Delta\dot{u} = \dot{u}_1 - \dot{u}_0; \qquad \Delta u = u_1 - u_0 \quad (4)$$

Newmark's first and second equations are defined by Eq. (5) and (6), respectively.

$$\dot{u}_1 = \dot{u}_0 + (1-\gamma) \times \Delta t \times \ddot{u}_0 + \gamma \times \Delta t \times \ddot{u}_1 \quad (5)$$

$$\Delta\ddot{u} = \frac{1}{\beta \times \Delta t^2} \times \Delta u - \frac{1}{\beta \times \Delta t} \times \dot{u}_0 - \frac{1}{2 \times \beta} \times \ddot{u}_0 \quad (6)$$

Substituting Newmark's first equation and considering an extended time-step length $\delta t = \theta \times \Delta t$ for Wilson's theta method, Eq. (3) becomes

$$m \times \left(\ddot{u}_0 + \delta\ddot{u}\right) + c \times \left(\dot{u}_0 + \delta t \times \ddot{u}_0 + \gamma \times \delta t \times \delta\ddot{u}\right) + \bar{k}_1 \times u_1 = p_{stat} + p_1 * \quad (7)$$

The equivalent load p_1* at the end of the time step is

$$p_1 * = p_1 \times \theta - p_0 \times (1-\theta) \quad (8)$$

The substitution of Eq. (6) and (8) into Eq. (7) and rearrangement in the matrix format yields the fundamental dynamic analysis equation implemented into the proposed method, as follows

$$\left[\left[k_{stat}\right] + \left[k_{dyn}\right]\right] \times \left\{u_1\right\} = \left\{p_{stat}\right\} + \left\{p_{dyn}\right\} \quad (9)$$

where

$$\left[k_{dyn}\right] = \frac{\left[m\right] + \left[c\right] \times \gamma \times (\theta \times \Delta t)}{\beta \times (\theta \times \Delta t)^2} \quad (10)$$

$$\left\{p_{dyn}\right\} = \left\{p_1 *\right\} + \frac{\left[m\right] + \left[c\right] \times \gamma \times (\theta \times \Delta t)}{\beta} \times \left[\frac{\left\{u_0\right\}}{(\theta \times \Delta t)^2} + \frac{\left\{\dot{u}_0\right\}}{(\theta \times \Delta t)} + \frac{\left\{\ddot{u}_0\right\}}{2}\right] - \left[c\right] \times \left\{\left\{\dot{u}_0\right\} + (\theta \times \Delta t) \times \left\{\ddot{u}_0\right\}\right\} - \left[m\right] \times \left\{\ddot{u}_0\right\} \quad (11)$$

Equation (9) makes it possible to perform dynamic analyses—based on a total-load secant-stiffness formulation—through the use of a static analysis method. Any of the three numerical analysis methods can be used by substituting γ = 1/2, β = 1/4, and θ = 1 for Newmark's average acceleration method; γ = 1/2, β = 1/6, and θ = 1 for Newmark's linear acceleration method; and γ = 1/2, β = 1/6, and θ = 1.42 for Wilson's theta method.

The nodal displacements are then calculated by solving the matrix equation as follows

$$\left\{u_1\right\} = \left[\left[k_{stat}\right] + \left[k_{dyn}\right]\right]^{-1} \times \left\{\left\{p_{stat}\right\} + \left\{p_{dyn}\right\}\right\} \quad (12)$$

The acceleration values at the end of the extended time-step length are calculated as

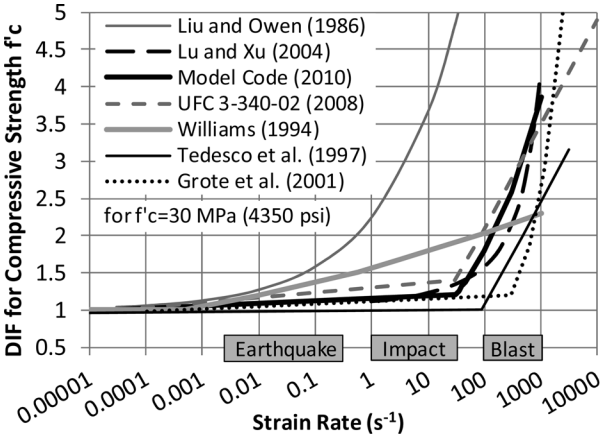

Fig. 2—Strain rate-DIF relationships for concrete strength.

$$\delta ii = \frac{u_1 - u_0}{\beta \times (\theta \times \Delta t)^2} - \frac{\dot{u}_0}{\beta \times (\theta \times \Delta t)} - \frac{\ddot{u}_0}{2 \times \beta} \tag{13}$$

The final accelerations, velocities, and displacements at the end of the actual time step—three values at each node—are then determined as follows

$$\ddot{u}_1 = \frac{\delta ii}{\theta} + \ddot{u}_0 \tag{14}$$

$$\dot{u}_1 = \Delta t \times \ddot{u}_0 + \gamma \times \Delta t \times \left(\ddot{u}_1 - \ddot{u}_0\right) + \dot{u}_0 \tag{15}$$

$$u_1 = \Delta t \times \dot{u}_0 + \frac{\Delta t^2}{2} \times \ddot{u}_0 + \beta \times \Delta t^2 \times (\ddot{u}_1 - \ddot{u}_0) + u_0 \tag{16}$$

SECTIONAL ANALYSES AND STRAIN RATE EFFECTS

The nonlinear sectional analysis formulations employed are as previously described in Guner and Vecchio (2010, 2011) for static loads. The only modification implemented in this study pertains to strain rate effects.

Numerous experimental studies have demonstrated that high rates of loading, such as those caused by impact or blast, result in increased strength in most materials. Although the reason for this increase is not entirely understood, it is widely considered to be a material property. Research studies conducted to date typically propose relationships between the dynamic increase factors (DIFs) and the strain rates for the concrete and reinforcing steel, where the DIF is the ratio of the dynamic to the static property of the material.

Several researchers have investigated the behavior of plain concrete under different rates of loading, including Liu and Owen (1986), Bischoff and Perry (1991), Williams (1994), Tedesco et al. (1997), Malvar and Ross (1998), Grote et al. (2001), and Lu and Xu (2004). In addition, UFC 3-340-02 (2008) and *fib* Model Code (2010) provide relationships. These studies typically contend that the concrete strength increases significantly under high rates of strain, as presented in Fig. 2, whereas the increase in the modulus of elasticity and the peak strain corresponding to the peak stress is relatively small.

The behavior of reinforcing steel under high loading rates has been investigated to a lesser extent. Formulations proposed by either CEB (1988) or Malvar (1998) have been commonly used in various numerical methods. In addition, Liu and Owen (1986), Filiatrault and Holleran (2002), UFC 3-340-02 (2008), and Asprone et al. (2009) provide DIF formulations or test data. These studies typically demonstrate that the yield stress is enhanced more significantly than the ultimate strength, as presented in Fig. 3. The rupture strain has been shown to be insignificantly affected while the modulus of elasticity is essentially unaffected by the rate of loading.

A small number of researchers contend that the material properties of concrete and reinforcing steel are independent of the loading rate. They attribute the apparent strength gain observed in the experiments to such factors as specimen geometry, inertial effects, and the boundary conditions imposed during testing. Among them are Li and Meng (2003), Georgin and Reynouard (2003), Cotsovos et al. (2009), and Zhang et al. (2009). Nonetheless, Cotsovos et al. (2009) acknowledges that the modification of static material properties for high rates of loading is a practical means for design purposes to account for this apparent strength gain, especially if the analysis method employed uses a lumped-mass approach.

In the proposed method, this apparent strength gain in the concrete and reinforcing steel is considered through the DIF approach. In this formulation, the strain rate values are calculated as defined in Eq. (17), where $\dot{\varepsilon}_1$ is the strain rate in the current time stage; ε_1 and ε_0 are the total strains in the current and previous time stages, respectively; and Δt is the time-step length.

$$\dot{\varepsilon}_1 = \left(\varepsilon_1 - \varepsilon_0\right) / \Delta t \tag{17}$$

Two strain rate values are calculated for each concrete layer using the principal tensile and compressive strains, and two strain rate values are calculated for the reinforcement using the total strains—one for each longitudinal steel layer and one for each smeared transverse steel component.

Once the strain rate values are determined, the corresponding DIFs are calculated for the modification of the static material properties. For concrete, the formulations proposed by the *fib* Model Code (2010) were implemented; these may be considered lower-bound values, as seen in Fig. 2. For both the longitudinal and transverse reinforcement, two different formulations were implemented: CEB

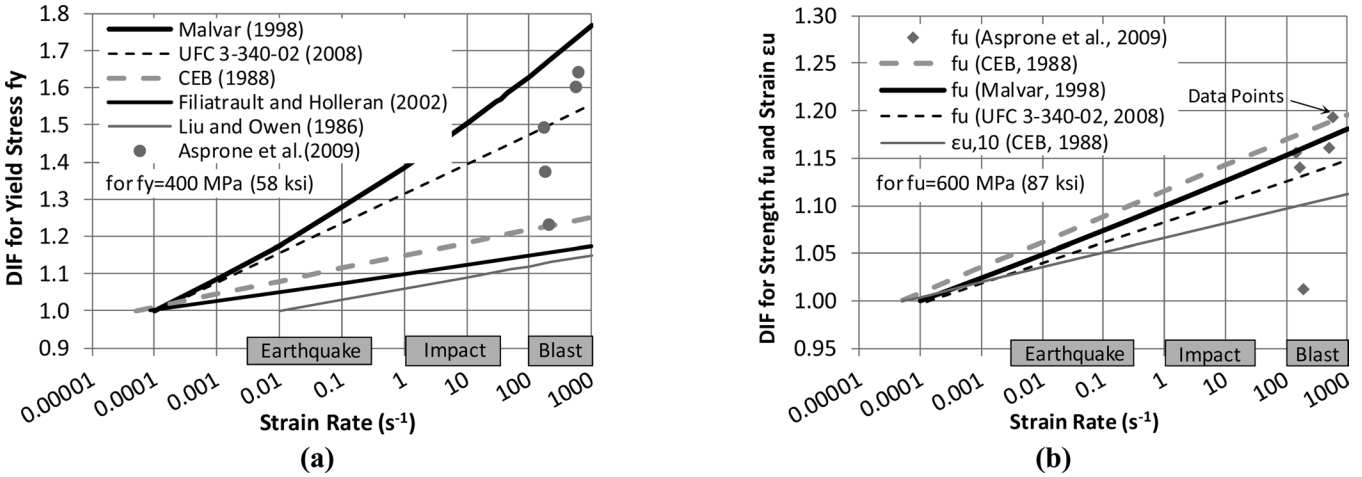

Fig. 3—Strain rate-DIF relationships for reinforcement in tension.

(1988) and Malvar (1998). Although both models propose similar increases for the ultimate strength, there is a considerable difference in their yield stress enhancements, as seen in Fig. 3. In the developed method, the Malvar (1998) formulations were selected as the default model to provide conservative response simulations for concrete- or shear-dominated behaviors. The lower-bound CEB (1988) formulations can also be used if deemed appropriate. Other, more comprehensive formulations can be implemented as they are developed in future studies.

APPLICATION TO BEAMS UNDER IMPACT LOADING

The beam specimens tested by Saatci and Vecchio (2009a), involving four pairs of beams subjected to a total number of 20 impact tests, were examined. All beams had identical geometry, test setup, and longitudinal reinforcement details, as shown in Fig. 4(a). The main variable was the amount of the transverse reinforcement. The concrete strengths also varied slightly, ranging from 44.7 to 50.1 MPa (6.5 to 7.3 ksi). The experimental program was comprised of Beams SS0a, SS0b, SS1a, SS1b, SS2a, SS2b, SS3a, and SS3b, where the numbers from 0 to 3 denote the transverse reinforcement ratios from 0.0 to 0.3%. The a-series and b-series beams were identical in all aspects except the loading protocol employed. The a-series beams were subjected to a drop mass of 211 kg (465 lb) in the first tests and 600 kg (1323 lb) in the second and third tests. The b-series beams were subjected to a drop mass of 600 kg (1323 lb) in the first and second tests and 211 kg (465 lb) in the third tests. All drop masses were released from a clear height of 3.26 m (10.7 ft) above the specimens, resulting in an impact velocity of 8.0 m/s (26.2 ft/s).

A frame model was created for one-half of each beam due to symmetry, as shown in Fig. 4(b). Member lengths were selected to be in the range of one-half the cross-section depth. A common difficulty in impact analysis modeling is the estimation of the impact load history, which requires several simplifications and assumptions; one such approach is proposed by CEB (1988). To eliminate this difficulty, the impacting mass was simulated in this study through a special modeling technique similar to that used by Saatci and Vecchio (2009b). For this, an artificial segment (Member 11 in Fig. 4(b)) was added to the model. This segment was assigned a very high stiffness to create a hard impact and a linear-elastic compression-only behavior to permit the separation of the drop mass from the beam after the impact. The drop mass was simulated by a lumped mass and placed at the top of Member 11, to which an initial velocity of 8.0 m/s (26.2 ft/s) was assigned to simulate the impact load. The self-mass of the beam was considered, with the values shown in Fig. 4(c).

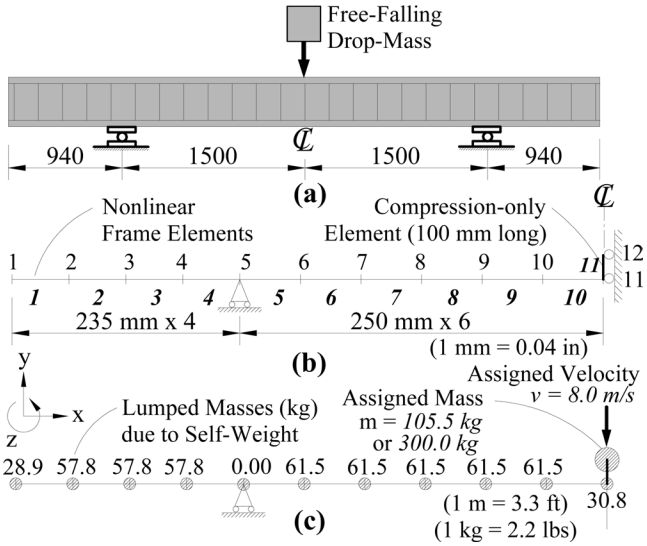

Fig. 4—SS beams: (a) dimensions and test setup; (b) frame model used; and (c) lumped masses and initial velocity loading used.

The sectional models were created using 32 concrete layers in a symmetrical layout (with concrete thicknesses of four layers of 7.75 mm [0.3 in.], two layers of 11 mm [0.4 in.], and 10 layers of 15.2 mm [0.6 in.]), and two steel layers, as shown in Fig. 5(a). Out-of-plane reinforcement ρ_z was smeared within a tributary area of five times the bar diameter d_{bz} (5 × 7.0 mm [0.3 in.] = 35 mm [1.4 in.]) at each side of the bar, as shown in Fig. 5(b). Transverse reinforcement ratios were assigned to all layers except the clear cover layers, with the ratios shown in Fig. 5(c). The concrete and steel properties used were as reported by Saatci and Vecchio (2009a), except the tensile strength of concrete, which was calculated using the lower-bound relationship $f_t' = 0.33 \times \sqrt{f_c'}$ (in MPa), as recommended by ACI 318-11 (ACI Committee 318 2011).

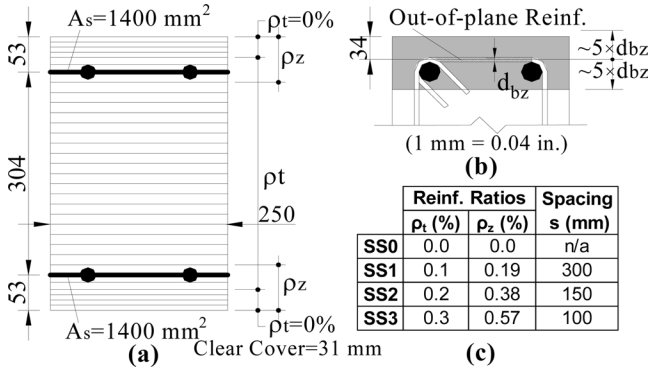

	Reinf. Ratios		Spacing
	ρ_t (%)	ρ_z (%)	s (mm)
SS0	0.0	0.0	n/a
SS1	0.1	0.19	300
SS2	0.2	0.38	150
SS3	0.3	0.57	100

Fig. 5—SS beams: (a) sectional models used; (b) determination of tributary area for out-of-plane reinforcement; and (c) smeared reinforcement ratios used. (Note: 1 mm^2 = 0.00155 in.^{2})

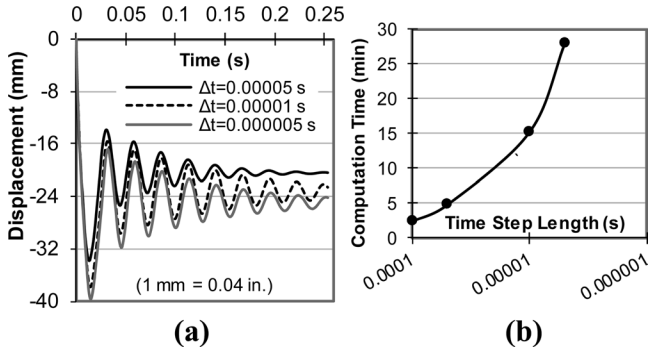

Fig. 6—Beam SS3b-1: (a) influence of time-step length on displacement response; and (b) computation time required.

Wilson's theta method, with no additional damping and a time-step length of 0.00001 seconds, was used in all analyses. The time-step length was determined as a result of multiple analyses, as presented in Fig. 6(a). The time-step lengths used in these analyses were selected in the order of the smallest natural vibration period of the beams (approximately 0.00003 seconds at the 21st mode). As seen in Fig. 6(b), the selection of an appropriate time-step length typically involves the determination of an optimum balance between the accuracy and the computation time.

Discussion of responses

The comparisons of the peak displacements and reactions, as obtained analytically and experimentally, are summarized in Table 1, where suffixes 1, 2, and 3 identify the test numbers. Example response comparisons for four tests are presented in Fig. 7; complete comparisons for all beams can be found in Guner (2008).

The peak displacements of the beams were calculated with good accuracy. Considering the 17 tests for which experimental peak displacement values were reported, a mean value of 0.99 and a coefficient of variation (COV) of 9.5% were achieved for the calculated-to-observed ratios. The peak displacements of previously damaged specimens were also calculated accurately. For the second and third analyses of the damaged beams (10 tests), the mean ratio and COV were 0.98 and 7.1%. Previously damaged specimens were analyzed in this study by storing the stress and strain histories in a data file and supplying it in the subsequent analysis.

Table 1—Comparison of analytical and experimental results

	Peak displacement, mm			Peak reaction, kN		
	Analysis	Test	Ratio	Analysis	Test	Ratio
SS0a-1	11.7	9.3	1.26	400.0	300.0	1.33
SS1a-1	10.3	11.9	0.87	416.5	356.4	1.17
SS2a-1	10.1	10.5	0.96	430.0	326.8	1.32
SS3a-1	10.0	10.6	0.94	442.3	398.0	1.11
SS0b-1	S.F.	S.F.	NA	504.3	399.8	1.26
SS1b-1	37.6	39.2	0.96	549.0	624.8	0.88
SS2b-1	37.4	37.6	0.99	621.6	592.5	1.05
SS3b-1	37.8	35.1	1.08	671.3	667.7	1.01
SS0a-2	S.F.	S.F.	NA	457.6	514.8	0.89
SS1a-2	38.8	39.3	0.99	564.0	510.0	1.11
SS2a-2	37.5	38.1	0.98	661.0	644.0	1.03
SS3a-2	38.1	36.8	1.04	703.0	802.0	0.88
SS1b-2	62.9	76.6	0.82	352.4	562.4	0.63
SS2b-2	58.6	61.5	0.95	498.0	621.0	0.80
SS3b-2	57.2	54.6	1.05	551.0	713.0	0.77
SS1a-3	64.5	NA	NA	346.5	503.0	0.69
SS2a-3	60.2	56.6	1.06	499.3	718.0	0.70
SS3a-3	58.7	57.0	1.03	577.0	689.0	0.84
SS2b-3	32.4	34.3	0.94	237.8	308.5	0.77
SS3b-3	28.7	30.4	0.94	286.0	344.9	0.83
A1-1	18.9	31.6	0.60	58.2	52.1	1.12
A1-2	136.0	124.4	1.09	87.0	94.0	0.93
A1-3	173.2	142.1	1.22	82.5	77.5	1.06
A1-4	122.4	107.2	1.14	62.9	73.4	0.86
A1-5	154.3	155.6	0.99	83.3	75.4	1.10
A1-6	146.9	175.5	0.84	81.2	73.4	1.11
A1-7	104.5	98.9	1.06	60.0	67.6	0.89
A1-8	145.1	199.6	0.73	77.8	62.0	1.25
B1-1	3.6	5.9	0.61	20.0	20.3	0.98
B1-2	13.9	13.3	1.04	40.0	33.0	1.21
B1-3	21.9	20.8	1.05	48.8	44.8	1.09
B1-4	32.5	37.7	0.86	51.4	66.4	0.77
B1-5	85.1	86.8	0.98	83.3	78.7	1.06
B1-6	119.2	150.3	0.79	91.3	119.2	0.77
B1-7	74.4	78.8	0.94	57.2	80.2	0.71
B1-8	127.0	133.1	0.95	95.7	132.7	0.72
B1-9	136.2	128.9	1.06	89.0	112.4	0.79
S1	74	89.4	0.83	217.4	200.4	1.08
		Mean	0.96		Mean	0.96
	%	COV	14.3		COV	19.2

Notes: NA is data not available due to faulty sensors; S.F. is shear failure; 1 mm = 0.04 in; 1 kN = 0.225 kips.

Given the scarcity of available tools for the analysis of previously damaged frames, the ability of the developed method to accurately capture the responses in the second and third impacts is noteworthy.

The peak support reactions of the beams were calculated with acceptable accuracy. Considering all 20 tests, a mean value

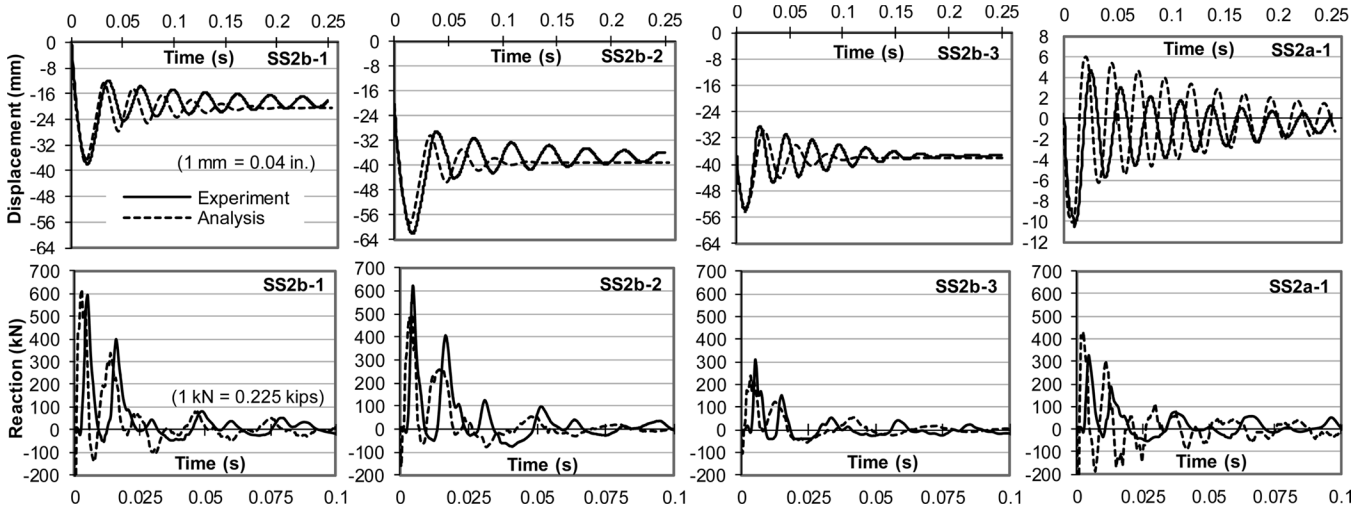

Fig. 7—SS beams: comparisons of midspan displacement and support reaction responses.

of 0.95 and a COV of 21.3% were achieved for the calculated-to-observed ratios. A general tendency in the analytical responses was to overestimate the peak reactions in the first tests and underestimate them in the second and third tests.

The post-peak damping characteristics of the beams were simulated with reasonable accuracy. For three of the beams (SS1a-1, SS3a-2, and SS3b-1), the damping of the displacement responses was captured with excellent accuracy; for 10 beams, the calculated displacement responses damped out slightly faster than the experimental responses, whereas for three beams (SS0a-1, SS2a-1, and SS3a-1), they damped out slower. Overall, there was a slight tendency in the analytical responses to dampen out more quickly than the experimental responses. This further justifies not using any additional viscous damping.

For Beams SS0 and SS1, the analytically determined crack widths, damage levels, and failure modes, when applicable, showed good correlation with the experimental observations. The analyses found shear-related mechanisms to be the major cause of the damage, consistent with the experimental observations. In the analysis, Beam SS0a-2 experienced an extensive shear failure involving Members 6, 7, 8, and 9, similar to the experimental observation shown in Fig. 8(a). On the other hand, the analytical shear failure of Beam SS0b-1 involved only Member 9, also similar to the experiment shown in Fig. 8(b). It is noteworthy that both Beams SS0 and SS1 were shear-critical under static load conditions; similarly, they exhibited shear-dominated behaviors under impact loads both in the experiments and in the analyses.

For Beams SS2 and SS3, the crack widths, dominant behavior, and damage levels were also calculated accurately. Analyses indicated flexure-dominated behaviors under the first impacts, as was observed in the experiment. For the second impacts, the analyses accurately calculated the shift in the behaviors toward shear cracking. For the third impacts, the experimental observation of no significant change in damage levels was also calculated. It is important to note that both Beams SS2 and SS3 were flexure-critical under static load conditions; when subjected to impact loads, however, they exhibited shear-related behaviors in the experiments and in the analyses. This demonstrates the need for employing analysis methods capable of considering shear effects when assessing structural performance under impact loads.

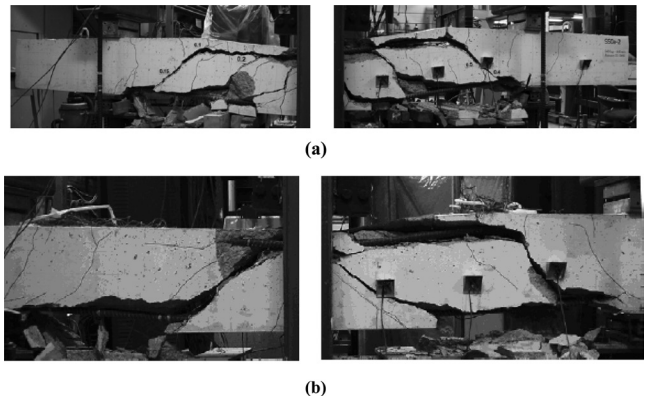

Fig. 8—Views of SS beams after tests: (a) SS0a-2; and (b) SS0b-1 (Saatci 2007).

Influence of strain rates

To assess the influence of the strain rate formulations implemented, a parametric study was conducted using the Malvar (1998) model, the CEB (1988) model, and no strain rate effects. In the analyses considering the stain rate effects, the *fib* Model Code (2010) formulations, the only available model implemented for the concrete, was used. As seen from a typical response comparison in Fig. 9, the consideration of strain rates only slightly affected the peak displacements, while a more significant influence was obtained for the residual displacements. The Malvar (1998) and CEB (1988) models resulted in a decrease in the peak displacements by approximately 8% and 5% and a decrease in the residual displacements by approximately 18% and 12%, respectively. The reaction responses were found to be insignificantly affected. As a result of this parametric study, it was concluded that the consideration of strain rates results in improvements in the calculated responses. Therefore, the formulations proposed by the Malvar (1998) model for the reinforcement and the *fib* Model Code (2010) for the concrete were selected as the default models and used throughout this study. Note that, in a seismic analysis, the effects of strain rates will typically be less significant than those from an impact or blast analysis.

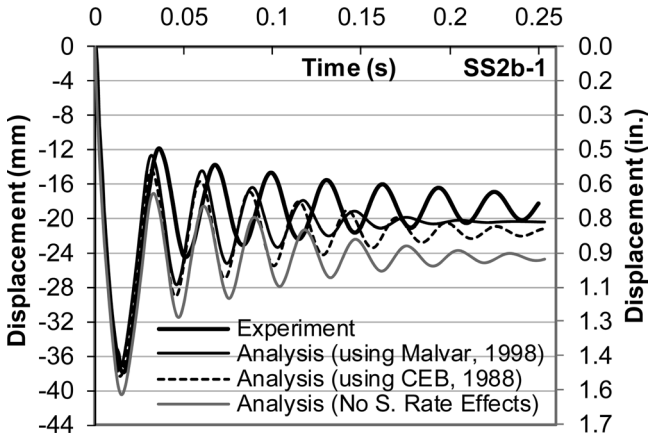

Fig. 9—Beam SS2b-1: Influence of strain rates on displacement response.

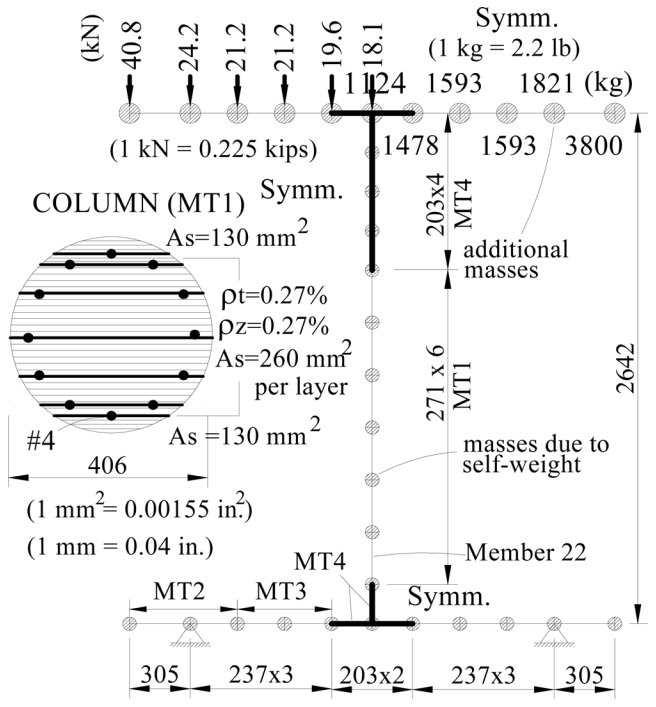

Fig. 10—Specimens A1 and B1: frame model used.

APPLICATION TO COLUMNS UNDER SEISMIC EXCITATION

The column specimens tested by Hachem et al. (2003), involving four 1/4.5-scale columns, were examined. All columns had identical cross sections and test setups, as shown in Fig. 10. The columns, constructed integrally with a square top slab and a footing slab, had well-confined circular cross sections with 1.20% longitudinal and 0.54% spiral reinforcement ratios, consistent with the modern design guidelines. The top slab carried three concrete blocks, resulting in a total mass of 29.5 tons (65 kips) supported by the column. The only difference between the specimens was the loading protocol employed. Specimens A1 and B1, which are examined herein, were subjected to unidirectional earthquake excitation, whereas A2 and B2 were subjected to bidirectional excitation. Specimen A1 was tested eight times, with each test (run) involving a scaled version of the Olive View record of the 1994 Northridge earthquake with the peak ground acceleration (PGA) values of 0.16, 0.58, 0.90, 0.60, 1.04, 1.02, 0.57, and 1.03 g, respectively. Specimen B1 was tested nine times subjected to the modified version of the Llolleo record of the 1985 Chile earthquake with the PGA values of 0.03, 0.08, 0.14, 0.19, 0.48, 0.87, 0.46, 0.89, and 0.91 g, respectively.

A frame model of the structure was created using member lengths in the range of one-half the cross-section depth. Stiffened end zones were used to account for the overlapping portions in the joint regions, as shown with bold lines in Fig. 10. The top slab was modeled at the elevation corresponding to the mass center of the top slab and the weight blocks. Three member types (MTs) were used to create the sectional models of the column and slabs; an additional MT was used for the stiffened joint members. Thirty-six concrete layers were used in the sectional model of the column, as shown in the inset of Fig. 10. In addition to the self-weight and self-mass of the structure, additional masses and gravity loads were applied to the top slab to consider the weight blocks. The acceleration history data used in all analyses were the ones recorded during the tests as the shake-table output. Wilson's theta method, with no additional damping and a time-step length of 0.0005 seconds, was used in all analyses. The ground motion applied to the specimens had a time interval of 0.01 seconds; therefore, each input time step was divided into 20 equal intervals in the analysis. The smallest natural vibration period of both specimens, at the 60th mode, was calculated to be 0.00011 seconds; therefore, the selected time-step length corresponds to 4.5 times the smallest period. For both specimens, it was confirmed that the use of a smaller time-step length did not significantly change the computed responses.

Discussion of responses

The peak base shear forces were calculated with good accuracy, as compared in Table 1. Considering all 17 analyses performed, a mean value of 0.97 and a COV of 17.5% were achieved for the calculated-to-observed ratios. As examples, the comparisons of base shear responses for Specimen A1 in Run 3 (maximum level) and Run 4 (design level) and for Specimen B1 in Run 3 (yield level) and Run 5 (design level) are shown in Fig. 11.

The peak deflection responses were also calculated reasonably well, as shown in Table 1. Considering all 17 analyses, a mean value of 0.94 and a COV of 17.8% were achieved for the calculated-to-observed ratios. The somewhat high scatter in the predictions was mainly caused by the earlier runs, where the analyses underestimated the peak displacements. Similar to the peak base shear forces, the peak deflections at design- and maximum-level earthquakes are typically the main focus in seismic performance assessments. When only the analyses involving the design- and maximum-level loading were considered (14 values), the mean and COV values became 0.98 and 13.8%, respectively. The representative displacement responses are presented in Fig. 11.

The post-peak damping characteristics of the columns were also captured reasonably well. As seen from Fig. 11, the slight tendency in the analytical responses was to dampen out more quickly than the experimental responses. Note that these analyses employ Wilson's theta method and do not use additional viscous damping. In the case of using Newmark's methods, which tend to require some additional damping for numerical stability, less accurate calculations would have been obtained. The vibration periods of the columns were calculated successfully with a slight underestimation.

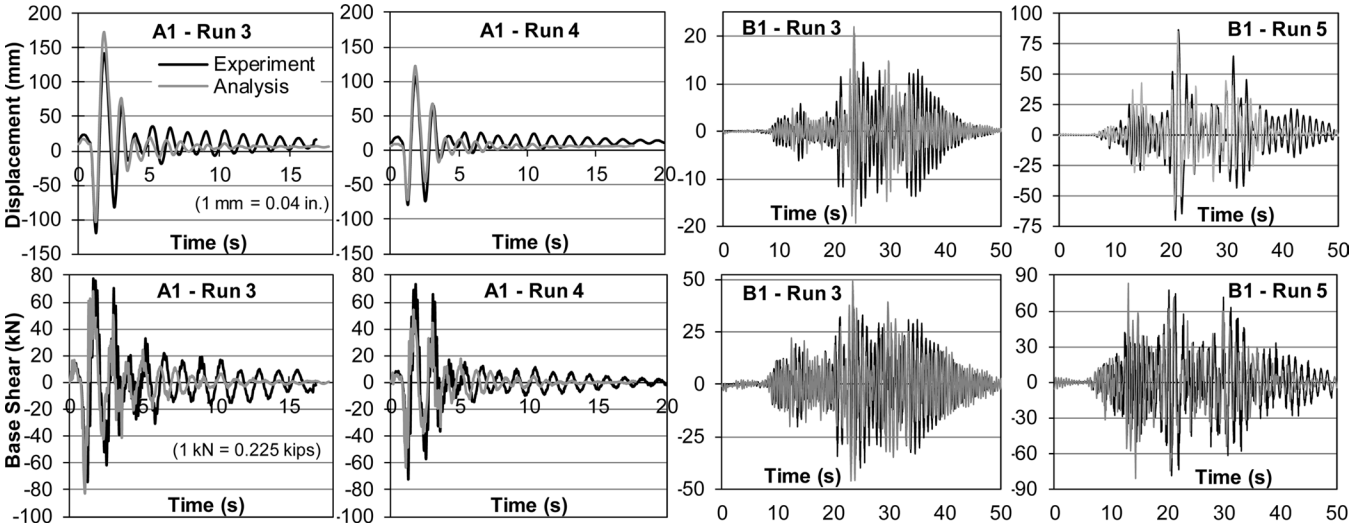

Fig. 11—Specimens A1 and B1: comparisons of displacement and reaction responses.

Considering all 17 analyses, a mean of 0.91 and a COV of 7.8% were obtained for the calculated-to-observed average periods. All columns exhibited flexural behaviors and damage modes in the analyses, which were consistent with the experimental observations.

APPLICATION TO FRAMES UNDER SEISMIC EXCITATION

The frame specimen tested by Elwood and Moehle (2003), involving a one-story, two-bay frame subjected to a modified version of the Villa del Mar record of the 1985 Chile earthquake with a PGA of 0.79 g, was examined. The frame consisted of two well-confined circular outer columns with 2.0% longitudinal and 2.9% transverse reinforcement ratios and one poorly confined square center column with 2.5% longitudinal and 0.18% wire transverse reinforcement ratios. The columns supported a 1537 mm (5 ft) wide and 343 mm (13.5 in.) deep beam, which represented the transfer beam of a seven-story building. The beam supported piles of steel weights, resulting in a total mass of 30.4 tons (67 kips), including the beam weight. Two identical frames were tested with the only difference being the special prestressing technique used for Specimen 2. Herein, only Specimen 1 is examined.

A frame model of the structure was created using member lengths in the range of one-half the cross-section depth. As is typical with frame analyses using line elements, stiffened end zones were used for the joint core regions, as shown with bold lines in Fig. 12. Four MTs were used for the sectional models of the top beam, columns, and footing beams; an additional four MTs were used for the stiffened joint zone members. In addition to the self-weight and self-mass of the structure, additional masses and gravity loads were applied to the top beam to simulate the steel blocks. The acceleration history data used in the analysis was the one recorded during the test as the table output. Wilson's theta method, with no additional viscous damping and a time-step length of 0.00025 seconds, was used in the analysis. The input accelerogram had time intervals of 0.01 seconds; therefore, each input time step was divided into 40 equal intervals. The smallest natural vibration period of the frame, at the 114th mode, was calculated to be 0.0000534 seconds; therefore, the selected time-step length corresponds to 4.7 times the smallest period. If the linear acceleration method had been used, a time-step length of less than

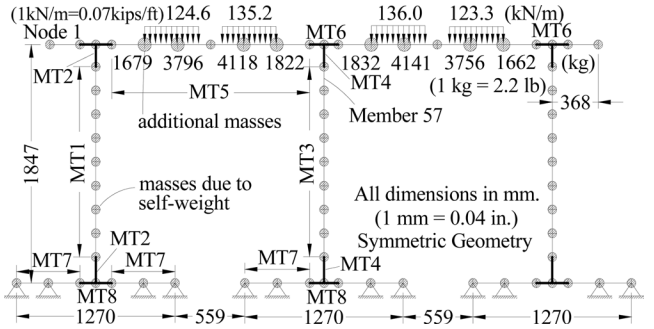

Fig. 12—Specimen 1: frame model used.

0.000029 seconds would have been required for numerical stability. The requirement of such an extremely small time-step length and excessive computation time demonstrates the importance of using an unconditionally stable integration method for the nonlinear seismic analysis of frames.

Discussion of responses

As seen in Fig. 13(a) and Table 1, the base shear response of the frame was captured accurately with a calculated-to-observed peak shear force ratio of 1.08. Furthermore, the damping of the base shear response showed strong similarities to the experimental response. As seen in Fig. 13(b), the lateral displacement response of the frame was calculated with acceptable accuracy, albeit with a discrepancy in the residual displacement. The peak deflection, calculated at Node 1 in Fig. 12, which occurred shortly after the shear failure of the center column, was calculated to be 0.83 times the experimental value. In the experiment, a considerable amount of reinforcement buckling took place in the central column after its shear failure, which caused an approximately 28 mm (1.1 in.) permanent lateral deflection, as seen in Fig. 13(b). The analysis method, however, does not currently consider reinforcement buckling, which caused the discrepancy in the displacement response beyond the time stage of 33.0 seconds.

In the analysis, the first significant cracking occurred at approximately 17.7 seconds at the top parts of all three columns. The center column suffered up to 0.8 mm (0.03 in.) wide shear cracks, while the outer columns experienced up to

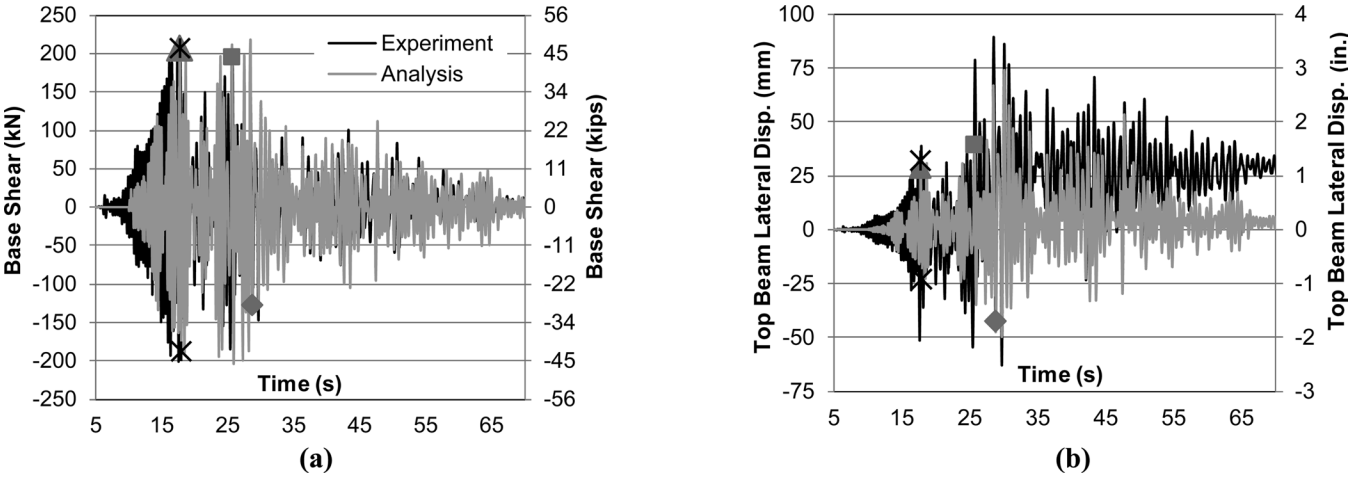

Fig. 13—Specimen 1: comparison of responses: (a) base shear; and (b) displacement.

2.0 mm (0.08 in.) wide flexural cracks. This time stage marked the first peak in the displacement response, shown with ▲ in Fig. 13(b). At approximately 25.7 seconds, the central column reached its shear capacity at Member 57. At this time stage, shown with ■ in Fig. 13, the shear crack widths of the central column reached 1.8 mm (0.07 in.), while the outer columns sustained 3.2 mm (0.13 in.) wide flexural cracks. At approximately 28.8 seconds, the analysis indicated the shear failure of the central column at Member 57 initiated by the fracture of its tie reinforcement. This time stage, shown with ◆ in Fig. 13, marked the start of significant deterioration of the frame's lateral stiffness and significant redistribution of the axial force from the central to outer columns.

The frame exhibited highly similar behavior in the experiment. The first major shear cracking was observed at the central column at 16.7 seconds; the shear capacity of the central column was reached at 24.9 seconds and the top portion of the center column failed in shear at 29.8 seconds. After this failure, significant spalling of the concrete and subsequent buckling of the longitudinal reinforcement at the top portion of the central column was observed. Also shown with × in Fig. 13 is the first yielding of the central column longitudinal reinforcement in the positive and negative loading directions, which correspond well with the experimental observations.

SUMMARY AND CONCLUSIONS

A recently developed static analysis method was further developed for a dynamic load analysis capability under impact, blast, and seismic loads. Newly developed and implemented formulations were presented. Among them are an explicit three-parameter time-step integration method and the consideration of the strain rate effects. The majority of structural damping is inherently considered through the realistic concrete and reinforcement hystereses used, eliminating the need to estimate a damping ratio for structural energy dissipation. Wilson's theta method was implemented to provide unconditional numerical stability even when no additional viscous damping is used. An approach was presented by which a static analysis method can be modified for a dynamic load analysis capability in a total-load secant-stiffness formulation. Furthermore, verification studies were undertaken using 11 previously tested specimens. The results of the studies conducted support the following conclusions:

1. Currently available dynamic analysis methods typically neglect shear effects despite the fact that various research studies and post-earthquake reconnaissance of frame structures have demonstrated the significance of shear effects under impact, blast, and seismic loads.

2. Newmark's and Wilson's theta methods can successfully be employed within a total-load secant-stiffness solution algorithm, resulting in excellent numerical stability.

3. Employing Newmark's linear acceleration method for a seismic time-history analysis becomes computationally prohibitive due to its extremely small time-step length requirement. Wilson's theta method permits the use of larger time-step lengths, thereby reducing the computational demand. Furthermore, it does not require the use of additional viscous damping for numerical stability, the determination of which is subjective and time-consuming.

4. The Palermo and Vecchio model for the concrete hysteresis and the Seckin model for the reinforcement hysteresis result in reasonably accurate simulations of the energy dissipation characteristics of frame members without requiring the use of additional viscous damping.

5. The disturbed stress field model, which uses a rotating smeared crack approach, can successfully be employed within a layered sectional analysis algorithm for the consideration of transverse shears in nonlinear dynamic analyses.

6. The use of dynamic increase factors (DIFs) in a nonlinear frame analysis using a lumped-mass approach provides improved response simulations—in particular, for impact loads. However, there are considerable discrepancies between the DIFs proposed by various researchers—in particular, with the yield stress DIFs for reinforcing bars.

7. Impact analyses can conveniently and accurately be performed through a modeling approach employing the impacting mass and the contact velocity. This eliminates complex pre-analysis calculations required to estimate the impact force history.

8. Multiple successive dynamic analyses can be successfully undertaken for previously loaded structures, taking previous damage into account.

9. The strategy adopted herein to modify an existing static analysis method for a dynamic load analysis capability, in a total-load secant-stiffness formulation, provides a convenient and viable platform for code development.

10. The developed analysis method accurately simulates the experimental responses of frames subjected to impact and seismic loads. Strengths, peak deflections, and damage and failure modes (including shear failures) are captured accurately. Considering all 38 simulations, mean values of 0.96 and 0.96 and COVs of 14.3% and 19.2% were obtained

for the calculated-to-observed peak-displacement and peak-reaction ratios, respectively. Computed parameters such as crack widths, reinforcement strains, and vibrational characteristics were also simulated well.

11. The developed analysis method exhibits excellent convergence and numerical stability, requiring a fraction of the analysis time demanded by micro finite element methods. Each impact analysis reported herein, for example, required approximately 15 minutes on a laptop computer.

12. Further work is required to consider reinforcement buckling behavior, found to be important in the behavior of certain structures. In addition, the implementation of a two-dimensional nonlinear joint model would eliminate the need, which may arise in some cases, to undertake detailed local analyses to determine the joint strength and ductility. Future work will be directed toward these areas and extending the method to three-dimensional frames.

ACKNOWLEDGMENTS

The authors would like to thank K. J. Elwood, M. M. Hachem, and S. Saatci for providing the experimental data for the specimens examined in this study.

REFERENCES

ABAQUS, 2010, "Analysis User's Manual Version 6.10," V. I to VI, ABAQUS, Inc. and Dassault Systémes, Providence, RI, 4515 pp.

ACI Committee 318, 2011, "Building Code Requirements for Structural Concrete (ACI 318-11) and Commentary," American Concrete Institute, Farmington Hills, MI, 503 pp.

Asprone, D.; Cadoni, E.; and Prota, A., 2009, "Tensile High Strain-Rate Behavior of Reinforcing Steel from an Existing Bridge," *ACI Structural Journal*, V. 106, No. 4, July-Aug., pp. 523-529.

Bischoff, P. H., and Perry, S. H., 1991, "Compressive Behaviour of Concrete at High Strain Rates," *Materials and Structures*, V. 24, No. 144, pp. 425-450.

CEB, 1988, "Concrete Structures under Impact and Impulsive Loading—Synthesis Report," Comité Euro-International du Béton, *Bulletin D'Information No. 184*, 184 pp.

Clough, R. W., and Penzien, J., 1993, *Dynamics of Structures*, second edition, McGraw-Hill, New York, 738 pp.

Cotsovos, D. M.; Stathopoulos, N. D.; and Zeris, C. A., 2009, "Behavior of RC Beams Subjected to High Rates of Concentrated Loading," *Journal of Structural Engineering*, ASCE, V. 134, No. 12, pp. 1839-1851.

CSI, 2006, "Perform3D: Nonlinear Analysis and Performance Assessment for 3D Structures—User Guide Version 4," Computers and Structures, Inc., Berkeley, CA, 336 pp.

El-Dakhakhni, W. W.; Changiz Rezaei, S. H.; Meeky, W. F.; and Razaqpur, A. G., 2009, "Response Sensitivity of Blast-Loaded Reinforced Concrete Structures to the Number of Degrees of Freedom," *Canadian Journal of Civil Engineering*, V. 36, No. 8, pp. 1305-1320.

Elwood, K. J., and Moehle, J. P., 2003, "Shake Table Tests and Analytical Studies on the Gravity Load Collapse of Reinforced Concrete Frames," *PEER Report 2003/01*, University of California, Berkeley, CA, 346 pp.

fib Model Code, 2010, "First Complete Draft, Volume 1, International Federation for Structural Concrete," *Bulletin* No. 55, Lausanne, Switzerland, Apr. 318 pp.

Filiatrault, A., and Holleran, M., 2002, "Stress-Strain Behavior of Reinforcing Steel and Concrete under Seismic Strain Rates and Low Temperatures," *Materials and Structures*, V. 34, No. 4, pp. 235-239.

Georgin, J. F., and Reynouard, J. M., 2003, "Modeling of Structures Subjected to Impact: Concrete Behaviour under High Strain Rate," *Cement and Concrete Composites*, V. 25, No. 1, pp. 131-143.

Grote, D. L.; Park, S. W.; and Zhou, M., 2001, "Dynamic Behavior of Concrete at High Strain Rates and Pressures: I. Experimental Characterization," *International Journal of Impact Engineering*, V. 25, No. 9, pp. 869-886.

Gunay, S. M., and Mosalam, K. H., 2010, "Structural Engineering Reconnaissance of the April 6, 2009, Abruzzo, Italy, Earthquake, and Lessons Learned," *PEER Report 2010/105*, University of California, Berkeley, CA, 46 pp.

Guner, S., 2008, "Performance Assessment of Shear-Critical Reinforced Concrete Plane Frames," PhD thesis, Department of Civil Engineering, University of Toronto, Toronto, ON, Canada, 429 pp., http://www.civ.utoronto.ca/vector/. (last accessed Aug. 4, 2012)

Guner, S., and Vecchio, F. J., 2008, "User's Manual of VecTor5," *Online Publication*, 88 pp., http://www.civ.utoronto.ca/vector/. (last accessed Aug. 4, 2012)

Guner, S., and Vecchio, F. J., 2010, "Pushover Analysis of Shear-Critical Frames: Formulation," *ACI Structural Journal*, V. 107, No. 1, Jan.-Feb., pp. 63-71.

Guner, S., and Vecchio, F. J., 2011, "Analysis of Shear-Critical Reinforced Concrete Plane Frame Elements under Cyclic Loading," *Journal of Structural Engineering*, ASCE, V. 137, No. 8, pp. 834-843.

Hachem, M. M.; Mahin, S. A.; and Moehle, J. P., 2003, "Performance of Circular Reinforced Concrete Bridge Columns under Bidirectional Earthquake Loading," *PEER Report 2003/06*, University of California, Berkeley, CA, 452 pp.

Li, B.; Huang, Z. W.; and Lim, C. L., 2010, "Verification of Nondimensional Energy Spectrum-Based Blast Design for Reinforced Concrete Members through Actual Blast Tests," *Journal of Structural Engineering*, ASCE, V. 136, No. 6, pp. 627-636.

Li, Q. M., and Meng, H., 2003, "About the Dynamic Strength Enhancement of Concrete-Like Materials in a Split Hopkinson Pressure Bar Test," *International Journal of Solids and Structures*, V. 40, No. 2, pp. 343-360.

Liu, G. Q., and Owen, D. R. J., 1986, "Ultimate Load Behaviour of Reinforced Concrete Plates and Shells under Dynamic Transient Loading," *International Journal for Numerical Methods in Engineering*, V. 22, No. 1, pp. 189-208.

LS-DYNA, 2010, "Keyword User's Manual," Version 971/Rev 5 (Beta), Livermore Software Technology Corporation, Livermore, CA, 2546 pp.

Lu, Y., and Xu, K., 2004, "Modelling of Dynamic Behaviour of Concrete Materials under Blast Loading," *International Journal of Solids and Structures*, V. 41, No. 1, pp. 131-143.

Malvar, L. J., 1998, "Review of Static and Dynamic Properties of Steel Reinforcing Bars," *ACI Materials Journal*, V. 95, No. 5, Sept.-Oct., pp. 609-614.

Malvar, L. J., and Ross, C. A., 1998, "Review of Strain-Rate Effects for Concrete," *ACI Materials Journal*, V. 95, No. 6, Nov.-Dec., pp. 735-739.

Newmark, N. M., 1959, "A Method of Computation for Structural Dynamics," *Journal of the Engineering Mechanics Division*, ASCE, V. 85, No. 3, pp. 67-94.

OpenSees, 2012, "Open System for Earthquake Engineering Simulation," Version 2.3.2, Pacific Earthquake Engineering Research Center, University of California, Berkeley, CA, http://opensees.berkeley.edu/wiki. (last accessed Aug. 4, 2012)

Palermo, D., and Vecchio, F. J., 2003, "Compression Field Modeling of Reinforced Concrete Subjected to Reversed Loading: Formulation," *ACI Structural Journal*, V. 100, No. 5, Sept.-Oct., pp. 616-625.

Rayleigh, Lord, 1877, *Theory of Sound*, V. 1, Dover Publications (1945), Mineola, NY, 504 pp.

Saatci, S., 2007, "Behaviour and Modelling of Reinforced Concrete Structures Subjected to Impact Loading," PhD thesis, Department of Civil Engineering, University of Toronto, Toronto, ON, Canada, 288 pp.

Saatci, S., and Vecchio, F. J., 2009a, "Effects of Shear Mechanisms on Impact Behavior of Reinforced Concrete Beams," *ACI Structural Journal*, V. 106, No. 1, Jan.-Feb., pp. 78-86.

Saatci, S., and Vecchio, F. J., 2009b, "Nonlinear Finite Element Modeling of Reinforced Concrete Structures under Impact Loads," *ACI Structural Journal*, V. 106, No. 5, Sept.-Oct., pp. 717-725.

Seckin, M., 1981, "Hysteretic Behavior of Cast-in-Place Exterior Beam-Column-Slab Subassemblies," PhD thesis, Department of Civil Engineering, University of Toronto, Toronto, ON, Canada, 236 pp.

SeismoStruct, 2010, "Finite Element Package for Space Frames under Static or Dynamic Loading," v5.2.2, SeismoSoft Ltd., Pavia, Italy, http://www.seismosoft.com. (last accessed Aug. 4, 2012)

Tedesco, J. W.; Powell, J. C.; Allen Ross, C.; and Hughes, M. L., 1997, "A Strain-Rate-Dependent Concrete Material Model for Adina," *Computers & Structures*, V. 64, No. 5-6, pp. 1053-1067.

UFC 3-340-02, 2008, "Structures to Resist the Effects of Accidental Explosions," Unified Facilities Criteria, U.S. Army Corps of Engineers, 1943 pp., http://www.wbdg.org/ccb/DOD/UFC/ufc_3_340_02_pdf.pdf. (last accessed Aug. 4, 2012)

Vecchio, F. J., 2000, "Disturbed Stress Field Model for Reinforced Concrete: Formulation," *Journal of Structural Engineering*, ASCE, V. 126, No. 9, pp. 1070-1077.

Williams, M. S., 1994, "Modeling of Local Impact Effects on Plain and Reinforced Concrete," *ACI Structural Journal*, V. 91, No. 2, Mar.-Apr., pp. 178-187.

Wilson, E. L.; Farhoomand, I.; and Bathe, K. J., 1973, "Nonlinear Dynamic Analysis of Complex Structures," *Earthquake Engineering & Structural Dynamics*, V. 1, No. 3, pp. 241-252.

Zhang, M.; Wu, H. J.; Li, Q. M.; and Huang, F. L., 2009, "Further Investigation on the Dynamic Compressive Strength Enhancement of Concrete-Like Materials Based on Split Hopkinson Pressure Bar Tests. Part I: Experiments," *International Journal of Impact Engineering*, V. 36, No. 12, pp. 1327-1334.